[33]J. J. Vuillemin, Phys. Rev. 144, 396 (1966).
[34]G. Williams, G. A. Swallow, and J. W. Loram, Phys. Rev. B 3, 3863 (1971).
[35]J. P. Burger, Ann. Phys. (Paris) 9, 345 (1964).
[36]G. A. Swallow, G. Williams, A. D. C. Grassie, and J. W. Loram, J. Phys. F 1, 511 (1971).
[37]G. G. Low and T. M. Holden, Proc. Phys. Soc. (London) 89, 119 (1966).
[38]G. Williams, Phys. Rev. B 5, 236 (1972).
[39]R. Schwaller and J. Wucher, Compt. Rend. B264, 1007 (1967).
[40]S. Skalski, M. P. Kawatra, J. A. Mydosh, and J. I. Budnick, Phys. Rev. B 2, 3613 (1970).
[41]O. Krogh Andersen, Phys. Rev. B 2, 883 (1970).
[42]That the s electrons dominate the conductivity in Pd appears reasonable in view of the analysis of Hall effect data (B. R. Coles, quoted in Ref. 11) on this metal which indicates that only 20% of the current is carried by d-band holes.
[43]M. P. Maley, R. D. Taylor, and J. L. Thompson, J. Appl. Phys. 38, 1249 (1967).
[44]T. A. Kitchens, W. A. Steyert, and R. D. Taylor, Phys. Rev. 138A, 467 (1965).
[45]H. Nagasawa, J. Phys. Soc. (Japan) 27, 787 (1969).
[46]We assume that internal fields (interactions) stabilize $\langle S_{\text{eff}}\rangle_{T_{\max}}$ at its $T_{\max}$ value for temperatures below $T_{\max}$.
[47]J. S. Dugdale and Z. S. Basinski, Phys. Rev. 157, 552 (1967).

PHYSICAL REVIEW B VOLUME 7, NUMBER 1 1 JANUARY 1973

Magnetic Moment, Susceptibility, and Electrical Resistivity of Dilute Paramagnetic Palladium–Rare-Earth Alloys*

R. P. Guertin†‡
Tufts University, Medford, Massachusetts 02155
and
H. C. Praddaude, S. Foner, and E. J. McNiff, Jr.
Francis Bitter National Magnet Laboratory,§ Massachusetts Institute of Technology, Cambridge, Massachusetts 02139
and
B. Barsoumian
Tufts University, Medford, Massachusetts 02155
(Received 26 July 1972)

The magnetic properties and low-temperature electrical resistivity are reported for dilute alloys of the $Pd_{1-x}R_x$ system where R = Ce, Pr, Nd, Sm, Eu, Gd, Tb, Dy, Ho, Er, Tm, Yb, Lu, or Y, and x is generally 0.01 or less. Alloys with R = Ce, Gd, Dy, or Er are examined over a wide range of concentrations. The quantities measured were the magnetic susceptibility $\chi(T)$ for $4.2 \lesssim T \lesssim 250$ K, the magnetic moment $\sigma(H_0)$ for $T \lesssim 4.2$ K and for $H_0 \lesssim 210$ kG, and the residual electrical resistivity $\rho(T)$ at 4.2 K. Even at 200 kG the rare-earth moments are not fully aligned with the applied field for $T \gtrsim 1.5$ K. The magnetic-moment versus field data are analyzed in two ways: by a semiempirical formula which includes a parameter that gives a convenient measure of ease of magnetic saturation of the rare-earth contribution, and by crystal field theory. Based on the semiempirical formula, the magnetic moment of the rare-earth ion is found to be close to its free-ion value, and the matrix susceptibility is also obtained. The application of the semiempirical formula to both field- and temperature-dependent data is discussed extensively. From recent electron-paramagnetic-resonance data, crystal field parameters for the $Pd_{1-x}Dy_x$ alloys are derived. Using these parameters, the field and temperature dependence of the magnetic moment for $Pd_{1-x}Dy_x$ are calculated. The best fit of crystal field theory shows large systematic deviations from experiment, whereas the semiempirical formula fits the observed data within experimental error for $H \gtrsim 3$ kG. The temperature-dependent susceptibility $\chi(T)$ is fitted to a Curie–Weiss law for the heavy rare-earth alloys and the free-ion value of the rare-earth moment is obtained within experimental error. The paramagnetic Curie temperature θ is less than ± 3 K for $x \lesssim 0.01$. The $\chi(T)$ data for R = Y, Ce, Eu, or Lu (none of which has a measurable moment in Pd) show that the position and magnitude of the maximum of $\chi(T)$ (which occurs at ~ 85 K for pure Pd) are sensitive functions of R and x. The analysis of the residual electrical resistivity of $Pd_{1-x}R_x$ alloys for $x \sim 0.01$ shows that the Kasuya formula does not apply. Other scattering mechanisms are suggested and their predictions are compared with the magnetic properties.

I. INTRODUCTION

In this paper we present a systematic analysis of an extensive series of experiments on the magnetic properties and the low-temperature electrical resistivity of paramagnetic $Pd_{1-x}R_x$ binary alloys. Here R = Ce, Pr, Nd, Sm, Eu, Gd, Tb, Dy, Ho, Er, Tm, Yb, Lu, or Y, and the concentration x is generally 0.01 or less.

Shaltiel and co-workers[1,2] have measured the

magnetic susceptibility and the rare-earth electron paramagnetic resonance (EPR) of several binary and ternary palladium–rare-earth alloys. The magnetic moment of $Pd_{1-x}Gd_x$ alloys for $0.01 \lesssim x \lesssim 0.05$ has been measured by Crangle.[3] Recently, EPR data of the UCLA[4] and University of Geneva[5,6] groups on very dilute alloys have been published. We have previously reported[7,8] isothermal magnetic-moment measurements in fields to 200 kG on some $Pd_{1-x}R_x$ alloys. Very few measurements of the low-temperature electrical resistivity of dilute $Pd_{1-x}R_x$ alloys have been reported[9,10]

From the magnetic data we find that in these dilute alloys all of the rare-earth ions have a 3+ valence, except Ce and Pr, which have a 4+ valence. Previously a moment of $1.1\mu_B$/Ce atom in Pd was reported[1]; we find less than $10^{-3}\mu_B$/Ce atom. For all our alloys, even at 210 kG, the rare-earth contribution is not saturated at 4.2 K. (Throughout the text we will use the expression "saturation of the rare-earth moment" to mean complete alignment of the moment with the applied field.) We find no evidence for the appreciable negative polarization of the conduction electrons previously reported in $Pd_{1-x}Gd_x$.[3]

This paper is organized as follows: In Sec. II we describe the sample-preparation techniques and the experimental details. In Sec. III the low-field magnetic susceptibility $\chi(T)$ for $4.2 \leq T \leq 250$ K is presented. The data are separated into two groups, those alloys where the rare earth shows a magnetic moment (Pr, Nd, Sm, Gd, Tb, Dy, Ho, Er, Tm, and Yb) and those alloys with no apparent rare-earth moment (Ce, Eu, Lu, and Y). In Sec. IV the high-field magnetic-moment data at 4.2 K and for applied fields H_0 up to 210 kG are presented. Analyses of the magnetic data using a semiempirical formula[11] and using crystal field theory are presented. In Sec. V the low-temperature electrical resistivity at zero magnetic field of all the $Pd_{1-x}R_x$ alloys for $x \sim 0.01$ is discussed. In Appendix A we discuss a search for the presence of the Pd_3R intermetallic phase in our alloys, and Appendix B contains a comparison of the magnetic properties of $Pd_{1-x}Er_x$ alloys prepared in different ways.

II. EXPERIMENTAL DETAILS

A. Sample Preparation

Most of the rare-earth elements make good dilute solid solutions with Pd, even though the usual Hume–Rothery rules are not strictly obeyed.[12] Our starting materials were of the highest purity available. The Pd (J&M wire) was better than 99.99% pure, and the rare-earth metals used were ~99.9% pure with respect to other rare-earth elements and were generally selected for low-Fe content. Since Fe impurities in Pd produce a giant moment ($\sim 10\mu_B$/Fe atom), significant amounts of Fe in the alloy could add a large spurious component to the magnetic moment of the impurity.

The constituents were arc melted in a gettered argon atmosphere on a water-cooled high-purity copper hearth. The first few melts were made at low current until it was clear that the rare-earth chip had melted into the host. Finally, the alloys were homogenized several times at high current and quenched to room temperature in about 1 sec. In most cases the weight losses assured ~3% accuracy of the nominal rare-earth concentration. In such cases the nominal concentration was assumed to be correct. Analyzed values were used when there were greater weight losses (i.e., for Eu, Tm, and Yb, which have low boiling points). Atomic absorption analysis was used to determine the rare-earth content to $\simeq \pm 10\%$.

The x-ray lattice spacings of several alloys were measured to search for the presence of any ordered intermetallic phases, such as Pd_3R. In particular, the lattice constant of our $Pd_{0.95}Gd_{0.05}$ alloy should be about 3.92 Å,[13] while Pd_3Gd, an ordered fcc structure of the Cu_3Au type, has a lattice constant of 4.08 Å.[14] No evidence of the Pd_3Gd phase was detected in this high-concentration alloy. The limits of resolution were such that if any Pd_3Gd were present, it would constitute less than about 1% of the sample. Other attempts to determine the presence of this intermetallic phase will be discussed in Appendix A.

B. Magnetic Measurements

Measurements of low-field ($H_0 \leq 17$ kG) susceptibility vs temperature were made with a vibrating-sample magnetometer (VSM) in an unshielded liquid-helium Dewar.[15] The liquid helium was allowed to boil away and the temperature drifted from 4.2 K to room temperature in 2 or 3 h. The magnetic moment at fixed field was measured during this warmup period. The applied field was small enough to ensure that the moment and field were linearly related. Thus, the measured moment was proportional to the "zero-field" susceptibility $\chi(T)$.

Magnetic-moment measurements in fields up to 50 kG were carried out with a commercial VSM and a superconducting magnet. These high-resolution measurements were used to normalize the moment-vs-field results made to ~210 kG with a very-low-frequency VSM[16] in water-cooled Bitter solenoids.

Several very dilute arc-melted and splat-cooled $Pd_{1-x}R_x$ samples ($x \leq 0.0025$) were furnished to us by Davidov, who had made EPR studies of the rare earths in some of these samples. We made magnetic measurements on these alloys and on similar

nonsplatted samples of our own in order to compare the magnetic properties of specimens prepared in different ways. These results are discussed in Appendix B.

C. Electrical-Resistivity Measurements

The electrical-resistivity (ρ) measurements were made on foils fabricated from chips of the same samples used in the magnetic measurements. The small chips were rolled to $\sim 3\times10^{-3}$ cm thickness and carefully cut into rectangles ~3 cm long and ~0.2 cm wide in a shearing device that cut both edges simultaneously. The foils were then etched and annealed at 500 °C for 4 h to remove strains introduced in the rolling process. The samples were immersed in a liquid-helium storage Dewar and the resistivity was determined from four-probe measurements by a method due to Loram *et al.*[17] In this way the absolute resistivity could be determined to about 1%.

III. TEMPERATURE DEPENDENCE OF MAGNETIC SUSCEPTIBILITY FOR $4.2 \leq T \leq 250$ K

A. Alloys with Large Rare-Earth Moments

The low-field temperature-dependent magnetic susceptibility $\chi(T)$ of an alloy of the $Pd_{1-x}Lu_x$ series was assumed to be equal to the matrix susceptibility $\chi_{mat}(T)$ and was subtracted from $\chi(T)$ of the $Pd_{1-x}R_x$ alloy to obtain the temperature-dependent rare-earth-ion susceptibility $\chi_R(T)$; i.e., $\chi_R(T) = \chi(T) - \chi_{mat}(T)$. The $\chi(T)$ for all the $Pd_{1-x}R_x$ alloys where R is nonmagnetic is shown in Fig. 1. For the Pd(Tm) and Pd(Yb) alloys the rare-earth content was estimated from weight losses in the arc-melting process and a linearly interpolated value of $\chi(T)$ for $Pd_{1-x}Lu_x$ was used for $\chi_{mat}(T)$.

In Figs. 2 and 3 we show $\chi_R^{-1}(T)$ vs T for most of the alloys studied, and $\chi(T)$ vs T is shown for two of them. The Curie law is well obeyed in all cases; i.e., $\chi_R^{-1}(T) \propto T$ for $T \gtrsim 20$ K. The rare-earth effective magnetic moment p_{Curie} (μ_B/atom) was deduced from the slope of the straight line drawn through the data points of Fig. 2 or Fig. 3 using the relation $\chi_R(T) = Np_{Curie}^2\mu_B^2/3kT$, where N is the number of rare-earth atoms per gram. The value of p_{Curie} is related to the high-field saturation moment p_{sat},

$$p_{Curie} = [(J+1)/J]^{1/2} p_{sat} , \quad (1)$$

where J is the total-angular-momentum quantum number.

The justification for using a Lu alloy as $\chi_{mat}(T)$ is that Lu, while not possessing a moment itself, is similar to the heavy rare earths in its chemical properties and presumably in its effect on the band susceptibility of Pd. Based on this assumption, only the effect of the impurity moment should be present in the $\chi_R^{-1}(T)$-vs-T plots; band filling or exchange enhancement alterations are assumed to be compensated for by the $\chi_{mat}(T)$ correction. If the susceptibility of Pd(Eu) or Pd(Ce) is used for $\chi_{mat}(T)$, there is less than 1% change in the value of p_{Curie} for the large-moment alloys. The straight lines in Figs. 2 and 3 appear to pass through the origin; the paramagnetic Curie temperature θ is less than about 2 or 3 K, where θ is deduced from a fit to the Curie–Weiss law $\chi(T) \propto (T \pm \theta)^{-1}$.

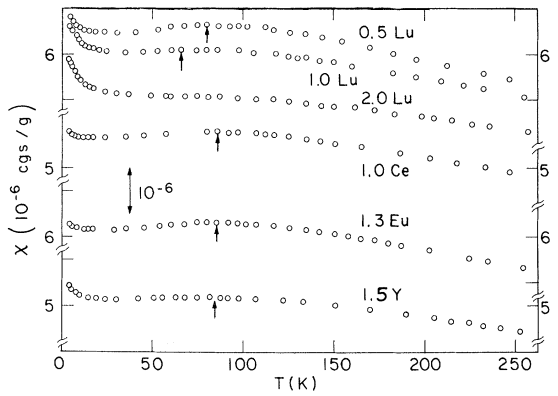

FIG. 1. Magnetic susceptibility $\chi(T)$ for $Pd_{1-x}R_x$ alloys where R = Lu, Ce, Eu, or Y (all of which have no magnetic moment in Pd). Concentrations are given in at. %. Note the ordinate axis breaks and the arrows which indicate the positions of the maxima in $\chi(T)$. The low-temperature increases in $\chi(T)$ are due to extraneous rare-earth and/or iron-group impurities.

The values of p_{Curie} derived from the data of Figs. 2 and 3 are tabulated in Table I with the values expected for the free-ion moment $g[J(J+1)]^{1/2}$, where the g factor and total-angular-momentum quantum number J for a 3+ ground-state rare-earth ion are used. Note that since $p_{Curie} \propto N^{-1/2}$, whereas $p_{sat} \propto N^{-1}$, any uncertainty in the exact concentration of R is less significant in evaluating p_{Curie} than p_{sat}. In all cases in Table I, except for Yb, the measured high-temperature moment is equal to the free-ion value within ± 5%. The results of similar measurements on the light rare-earth alloys (e.g., Pr, Nd, and Sm) are not included in this tabulation because the rare-earth moments are very small and the choice of $\chi_{mat}(T)$ becomes an important contribution to the value of p_{Curie}.

We note from Figs. 2 and 3 that $\chi_R^{-1}(T)$ vs T is quite linear at high T for all the heavy rare-earth alloys, even though contributions from $\chi_{mat}(T)$ are more significant. If there were excited states at energies within a few hundred degrees of the ground-state manifold, we would expect deviations from the Curie-law behavior at higher temperatures. Previous investigations[18] show that for the heavy rare earths listed in Table I there are no

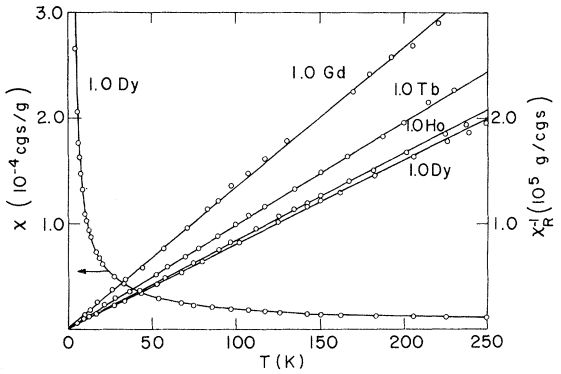

FIG. 2. Inverse of the rare-earth contribution to the susceptibility $\chi_R^{-1}(T)$ for $Pd_{1-x}R_x$ alloys where R = Gd, Tb, Ho, or Dy, and $\chi(T)$ for $Pd_{0.99}Dy_{0.01}$. Here $\chi_R(T) = \chi(T) - \chi_{mat}(T)$, where $\chi_{mat}(T)$ is the susceptibility of $Pd_{0.99}Lu_{0.0}$ (see Fig. 1). The slope of $\chi_R^{-1}(T)$ vs T determines the effective moment per R atom listed in Table I.

excited states lying below ~1400 K.

Crystal field effects can produce deviations from the Curie law at low temperatures. Such effects have been observed by Williams and Hirst[19] for dilute $Au_{1-x}R_x$ and $Ag_{1-x}R_x$ alloys. In contrast, we observe only slight deviations from the Curie law in the $Pd_{1-x}R_x$ alloys. In Sec. IV B we discuss the effects of crystal fields on the high-field magnetic-moment data of $Pd_{0.99}Dy_{0.01}$ at 4.2 K and on $\chi_R(T)$.

B. Alloys with Zero Rare-Earth Moment

We have found that dilute amounts of Y, Lu, Ce, and Eu do not show a magnetic moment when dissolved in Pd. The zero moment for Y and Lu is expected, but Ce or Eu may or may not have a moment depending on the valence state of Ce or Eu in the matrix. Our data indicate that Ce goes into solution as Ce^{4+}, and Eu goes into solution as

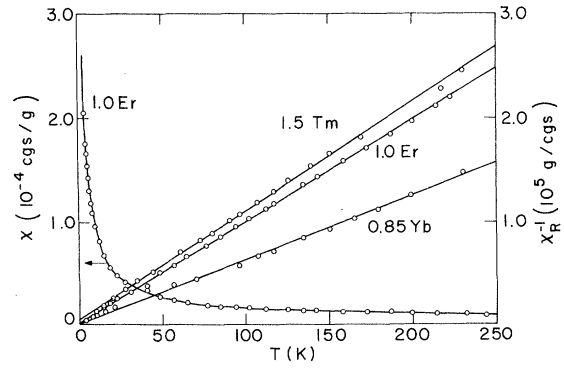

FIG. 3. Inverse rare-earth contribution to the susceptibility $\chi_R^{-1}(T)$ for $Pd_{1-x}R_x$ alloys where R = Tm, Er, or Yb, and $\chi(T)$ for $Pd_{0.99}Er_{0.01}$. The symbols are defined in the caption of Fig. 2.

TABLE I. Effective moment p_{Curie} (μ_B/atom) for heavy rare earths in $Pd_{1-x}R_x$ determined from low-field susceptibility measurements $\chi(T)$ for $4.2 \le T \le 250$ K. The free-ion R^{3+} moment is given in column 4.

R	Conc. (at.%)	p_{Curie}	$g[J(J+1)]^{1/2}$
Gd	1.00	7.9	7.94
Tb	1.00	9.2	9.72
Dy	1.05	10.3	10.65
Ho	1.00	10.1	10.18
Er	1.00	9.3	9.58
Tm	1.50	7.2	7.56
Yb	0.85	4.0	4.54

Eu^{3+}. Based on high-resolution $\sigma(H_0)$ measurements of $Pd_{0.99}Ce_{0.01}$ we can place an upper limit on the moment of Ce in Pd as less than $10^{-3}\mu_B$/Ce atom. Earlier data[1] suggested $1.1\mu_B$/Ce atom.

In Fig. 1 we plot $\chi(T)$ for three Pd(Lu) samples and also for $Pd_{0.985}Y_{0.015}$, $Pd_{0.987}Eu_{0.013}$, and $Pd_{0.99}Ce_{0.01}$. The small increases in $\chi(T)$ at low T are probably due to trace amounts of Fe (~20 ppm) and/or other rare-earth impurities in the alloys. Several other $Pd_{1-x}Ce_x$ alloys with $0.002 \le x \le 0.07$ have been studied. The results are similar to the $x = 0.01$ alloy but the Ce used for these alloys was of lower purity and, as expected, the low-temperature $\chi(T)$ increases are larger. The low-temperature increase in $\chi(T)$ for the $Pd_{0.93}Ce_{0.07}$ alloy was greater than could be accounted for by Fe, Co, or extraneous R impurities. This may be an indication that the effective Ce valence is less than 4+ at high concentrations, perhaps because of Ce-Ce interactions.

In Fig. 4 we show the high-field susceptibility χ_{HF} at 50 kG and 4.2 K vs concentration for all the alloys showing no magnetic moment. It is evident

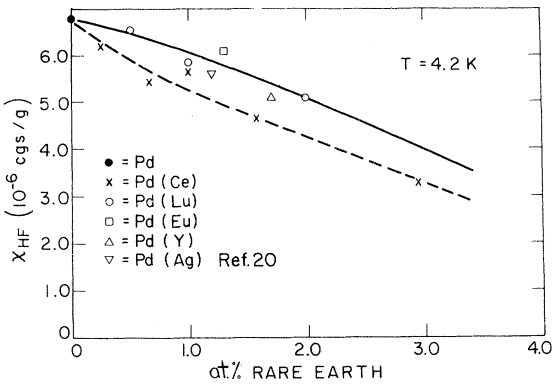

FIG. 4. Susceptibility χ_{HF} at 50 kG and 4.2 K vs concentration for the $Pd_{1-x}R_x$ alloys where R has zero magnetic moment in Pd. The solid curve is drawn for R^{3+} rare-earth ions and the dashed curve is for R^{4+} (i.e., R = Ce).

that χ_{HF} decreases somewhat more rapidly per Ce atom than for other rare earths. This is not surprising because we would expect Ce^{4+} to furnish an additional electron to the conduction band compared to the 3+ ions, and the large susceptibility of Pd is expected to be a sensitive function of conduction-electron concentration. For comparison, the concentration dependence of χ_{HF} for Pd(Ag) is also shown in Fig. 4.

Returning to Fig. 1, careful examination of the shape of the curves reveals an interesting effect: The position of the maximum of $\chi(T)$ depends on x and R (see arrows). When Lu is added to Pd, the maximum $\chi_{mat}(T)$ shifts toward lower temperatures, whereas for all the other alloys discussed in this paper the maxima remain at 85 K. The temperature T_{max} vs concentration of rare earth is plotted in Fig. 5, where T_{max} is the temperature at which χ_{max} occurs. The shift of $\chi_{max}(T)$ toward $T=0$ for Pd(Lu) is similar to that for Pd(Rh).[20] The gradual decrease in the magnitude of χ_{max} at 85 K with increasing concentration of rare earth is characteristic of the Pd(Ag) alloys.[20] The difference between the two cases is quite striking.

Several explanations for the existence of the susceptibility maximum in Pd have been advanced.[21-27] None of these models fully accounts for $\chi(T)$ of Pd and its alloys. It seems clear that the position, and indeed the existence of $\chi_{max}(T)$ depends strongly on both the topology of the Fermi surface and the exchange enhancement. It is hoped that our results for dilute rare-earth alloys of Pd will motivate further theoretical work on the susceptibility anomalies in strongly paramagnetic metals and alloys.

IV. FIELD DEPENDENCE OF MAGNETIC MOMENT AT LOW TEMPERATURES ($0 \leq H_0 \leq 200$ kG)

A. Experimental Results

The magnetic moment $\sigma(H_0)$ in $Pd_{1-x}R_x$ alloys where R = Y, Ce, Eu, or Lu (all have zero moment in Pd) was measured to either 150 or 200 kG at 4.2 K. No deviations from linearity of $\sigma(H_0)$ vs H_0 were detected. This is reasonable since $\chi_{HF} < \chi_{HF}$(Pd) (see Fig. 4). In contrast, in higher-susceptibility alloys, e.g., $Pd_{1-x}Rh_x$, field-dependent Pauli paramagnetism is observed.[28]

The $\sigma(H_0)$ isotherms at 4.2 K for the $Pd_{1-x}R_x$ alloys, where R is a rare earth with a nonzero moment, are plotted in Figs. 6 and 7. In all cases the rare-earth moment is not saturated even at 200 kG. Lowering the temperature to 1.5 K has little effect on the approach to saturation. It is clear that some means (e.g., a functional dependence) of extrapolating the data to higher fields is necessary in order to extract the saturation magnetic moment of the rare earth and the value of the matrix susceptibility.

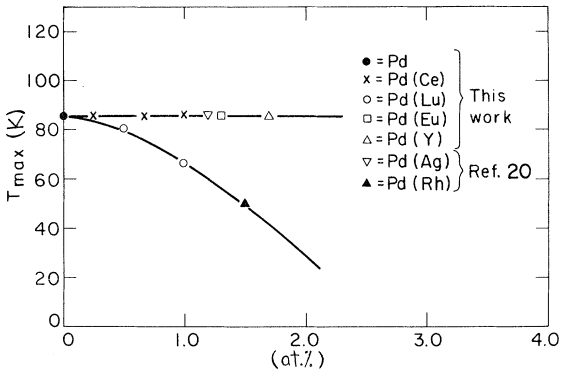

FIG. 5. Temperature of the susceptibility maximum T_{max} vs concentration of solute for $Pd_{1-x}R_x$ alloys where R has no moment in Pd. $Pd_{1-x}Lu_x$ and $Pd_{1-x}Rh_x$ show a rapid variation of T_{max} vs concentration.

B. Analysis of Magnetic-Moment Data

1. Application of Semiempirical Formula

Praddaude[11] has developed a semiempirical formula which fits all the high-field data to better than ~1%. For fixed temperature this formula is

$$\sigma(H_0) = \frac{AH_0}{1+B|H_0|} + CH_0 \ . \tag{2}$$

The first term on the right-hand side describes the field dependence of the moment (here a rare earth) and it is the simplest rational Padé approximant. In the limit of large H_0, Eq. (2) becomes $A/B + CH_0$, so that C is just the matrix susceptibility and A/B is proportional to p_{sat} (μ_B/atom), the saturation moment per rare-earth atom. In the limit of small H_0, Eq. (2) approaches $(AH_0 + CH_0)$; thus A is a measure of the low-field rare-earth susceptibility. The parameter B is a measure of the the ease of saturating the rare-earth moment; large B means saturation is readily achieved. A discussion of Eq. (2) and its application to the $Pd_{1-x}R_x$ system has been given in Refs. 7, 8, and 11. We will illustrate here the utility of Eq. (2) for studying the magnetic properties of the $Pd_{1-x}R_x$ system by examining its application to a particular alloy, $Pd_{0.98}Gd_{0.02}$.

a. Field dependence of σ for $Pd_{0.98}Gd_{0.02}$. A fit of Eq. (2) to the $\sigma(H_0)$ data up to 212 kG for $Pd_{0.98}Gd_{0.02}$ at 4.2 K is shown in Fig. 8. For a free Gd ion the variation of σ vs H_0 is given by a Brillouin function $B_J(gJ\mu_B H_0/kT)$, where $J=\frac{7}{2}$ and $g=2$ for Gd^{3+}. Even when an effective temperature $(T-\theta)$ is included in the argument of $B_{7/2}$ corresponding to a Gd-Gd interaction of $\theta = +1.5$ K (where θ is optimized for the best fit to the data), the data points and the modified Brillouin function still show large and systematic deviations (see Fig. 8). Such large deviations also are found for

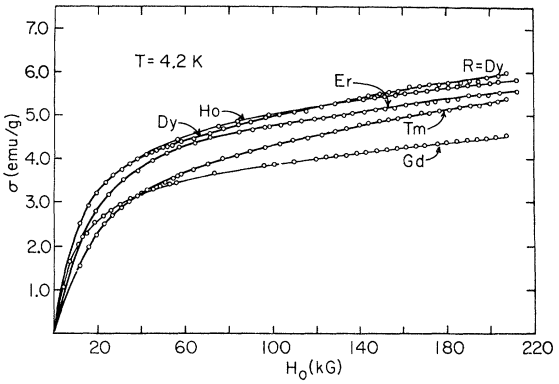

FIG. 6. Magnetic moment vs applied field at 4.2 K for $Pd_{1-x}R_x$ alloys where R = Gd, Tb, Dy, Ho, Er, or Tm. The solid lines represent the best fit to the data by Eq. (2).

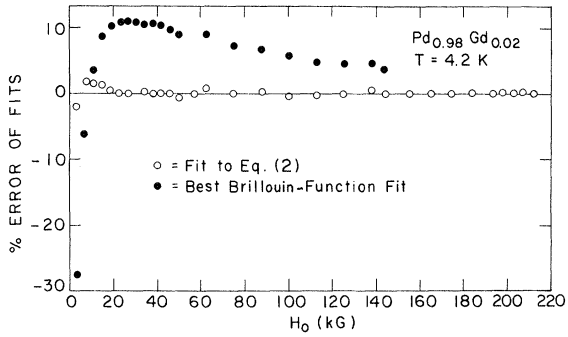

FIG. 8. Comparison of best fits by Eq. (2) and of a Brillouin function to the magnetic moment of $Pd_{0.98}Gd_{0.02}$ at 4.2 K. The fit to the Brillouin function is for $B_{7/2}[7\mu_B H_0(T-1.5)]$. The percent deviation of the fits is shown as a function of H_0. The deviations from the Brillouin-function fit are large and systematic, whereas the deviations from the fit to Eq. (2) are small and random.

B_J, where $J=\frac{1}{2}$, 3, 4, $\frac{9}{2}$, or 5. On the other hand, the fit of Eq. (2) to the data is well within 1% over the field range $3.18 \leq H_0 \leq 212$ kG and there are no systematic deviations at low or high fields. Clearly, the semiempirical formula gives a remarkable description of the field dependence of $\sigma(H_0)$ at fixed T. Equally good fits were obtained for data taken at $T=14$, 20, and 30 K over the field range $3.8 \leq H_0 \leq 50$ kG.

b. Temperature dependence of σ for $Pd_{0.98}Gd_{0.02}$. If Eq. (2) reflects an adequate mathematical description of $\sigma(H_0)$, we expect it to yield a reasonable description of the temperature dependence of σ. The temperature dependence of A and B must be identical since the moment A/B is assumed to be a constant, independent of H_0 and T. Assuming $A=a/(T-\theta)$ and $B=b/(T-\theta)$, i.e., A and B each follow a Curie–Weiss law, the best value of θ is obtained from the $\sigma(T)$ data at fixed H_0. Data at $H_0=12.5$ and 50 kG for $4.2 \leq T \leq 300$ K for the $Pd_{0.98}Gd_{0.02}$ sample were employed, and a value of $\theta = 4.0 \pm 0.2$ K was obtained. The calculated and measured values of the moment agree within 6% from 250 down to 6 K. However, the deviations are systematic and outside the experimental error. A fit of the usual Curie–Weiss law shows that large systematic deviations occur for $T \lesssim 30$ K. It should be noted that the B term in the denominator of Eq. (2) introduces a field dependence not present in the usual Curie–Weiss law. When $H_0 \to 0$, the temperature-dependent form of Eq. (2) reduces to the usual Curie–Weiss law. Finally, a general form of A and B varying as $(T-\theta)^{-\alpha}$ was examined, and $\alpha = 1.1$ generated the best fit to the data. However, the improvement over the $\alpha = 1$ fit was negligible.

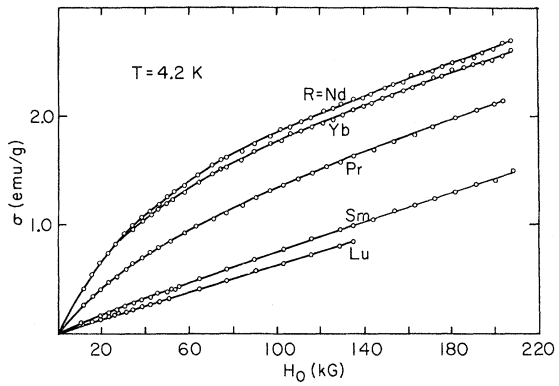

FIG. 7. Magnetic moment vs applied field at 4.2 K for $Pd_{1-x}R_x$ alloys where R = Nd, Yb, Pr, Sm, or Lu. The solid lines represent the best fit of the data by Eq. (2).

c. Approach to saturation of the rare-earth ion. We return now to the B term of Eq. (2) and treat it as a temperature-independent parameter. B is a measure of the ease of magnetizing the rare-earth moment or, alternatively, a way to include the field dependence of σ to lowest order. To illustrate the effect of B on $\sigma(H_0)$, we show in Fig. 9 plots of the normalized magnetic moment vs field to $H_0 = 200$ kG for different values of B. The quantity of importance is the magnitude of $B|H_0|$ compared to 1. When $B|H_0| \sim 20$, 95% of saturation is achieved. Hence, Fig. 10 can be used as a guide to determine if sufficient field is available to deduce p_{sat} ($\propto A/B$) and $\chi_{mat} = C$. It is important to realize that in order to evaluate A/B accurately from the high-field extrapolation the contribution of the C term of Eq. (2) must be small. This means that at low fields C cannot be deduced unless one has extremely accurate $\sigma(H_0)$ data as well as a good functional dependence, such as Eq. (2).

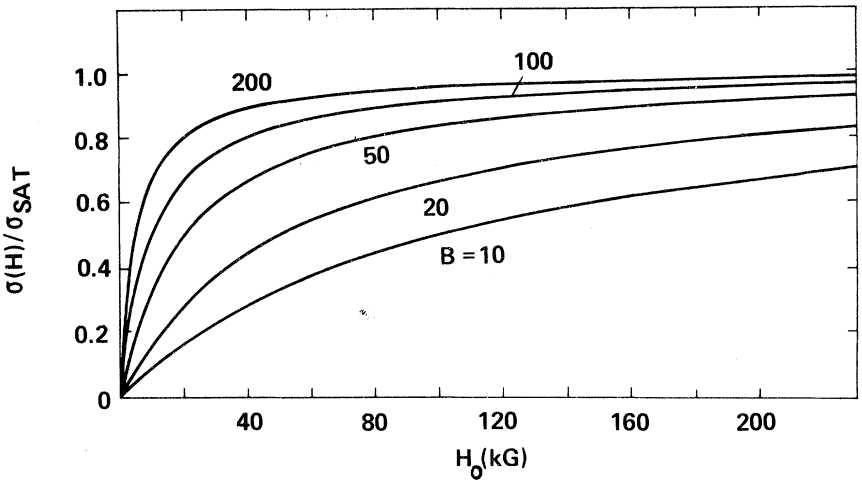

FIG. 9. Several normalized plots of the magnetic moment vs H_0 for Eq. (2), where $C=0$. The units of the parameter B are $(10^6\ \mathrm{G})^{-1}$ When $B\,|H_0| \sim 20$, saturation is $\sim 95\%$ complete at 200 kG.

For this reason we attempt to get as near to magnetic saturation as possible before analyzing the data.

Several approaches can be used to examine the extrapolation of the data to high fields. One approach is to fit Eq. (2) to data in different field ranges and to compare how A/B and C change. In Table II we have listed the parameters B, C, and p_{sat} ($\propto A/B$) of Eq. (2) for $Pd_{0.98}Gd_{0.02}$ and field ranges 0–50, 0–150, and 0–210 kG. In this case the parameters do not change significantly as higher-field data points are added. All the other rare-earth alloys are less easily magnetized; for these such comparisons are poorer.

d. Application to $Pd_{1-x}R_x$ alloys. In Table III we list at 4.2 K the $\sigma(H_0)$ data of all the $Pd_{1-x}R_x$ alloys and their corresponding C, B, and p_{sat} parameters. Within our accuracy in determining the rare-earth concentration, we see that the high-field moment in each case is equal to the free-ion value gJ. All the rare-earth ions appear to go into solution as R^{3+} except for Ce and Pr, which go in as R^{4+}. These results, then, are in general agreement with those of Table I when the relation between p_{sat} and p_{Curie} is used [Eq. (1)]. The values of C for most of the alloys are consistent with that of $Pd_{1-x}Lu_x$ for the same range of concentration. This supports our use of $Pd_{1-x}Lu_x$ for the evaluation of χ_{mat} in Sec. III A.

TABLE II. Comparison of the best fits of Eq. (2) for the $\sigma(H_0)$ data of $Pd_{0.98}Gd_{0.02}$ at 4.2 K for three different ranges of applied field.

Field range (kG)	B $(10^6\ \mathrm{G})^{-1}$	C $(10^{-6}/\mathrm{g})$	$p_{\mathrm{sat}}(\propto A/B)$ (μ_B)
0–50	179	11.1	6.4
0–150	158	3.54	6.8
0–210	161	3.61	6.8

Qualitatively, the variation of B from rare earth to rare earth appears to follow the relative magnitude of the ratio of the total to the orbital angular momentum of the rare-earth ion. Thus Gd, which has $L=0$, has a rather large B (is relatively easy to magnetize), whereas Ho ($J=8$ and $L=6$) is more difficult to magnetize. This argument also applies when one compares the heavy and light rare-earth ions.

2. *Application of Crystal Field Theory*

In Sec. IV B 1 d we discussed the analysis of the magnetic data using Eq. (2). Although Eq. (2) fits our data remarkably well, the lack of theoretical support for this formula is a bothersome shortcoming. In this section we discuss the application of crystal field theory to our data.

a. Crystal field Hamiltonian. In the last two years EPR has been observed for several rare-earth ions in single crystals of Al, Ag, Au, Pt, and Pd [4–6, 29] and the results have been interpreted using crystal field theory. The $2J+1$ degeneracy of the ground-state levels of the rare-earth ions is partially lifted by the cubic crystal field of the host. Following the notation of Lea, Leask, and Wolf,[30] the Hamiltonian of a rare-earth ion in a cubic crystalline field is

$$H_{\mathrm{CF}} = B_4 O_4 + B_6 O_6 , \tag{3}$$

where O_4 and O_6 are the fourth- and sixth-order cubic crystal field operators and B_4 and B_6 are the respective strengths of the perturbation. The above expression assumes that the z axis is taken along a fourfold-symmetry axis. Following Ref. 30, it is convenient to introduce the notation

$$F_4 B_4 = Wx , \quad F_6 B_6 = W(1 - |x|) , \tag{4}$$

where F_4 and F_6 are coefficients that depend on the

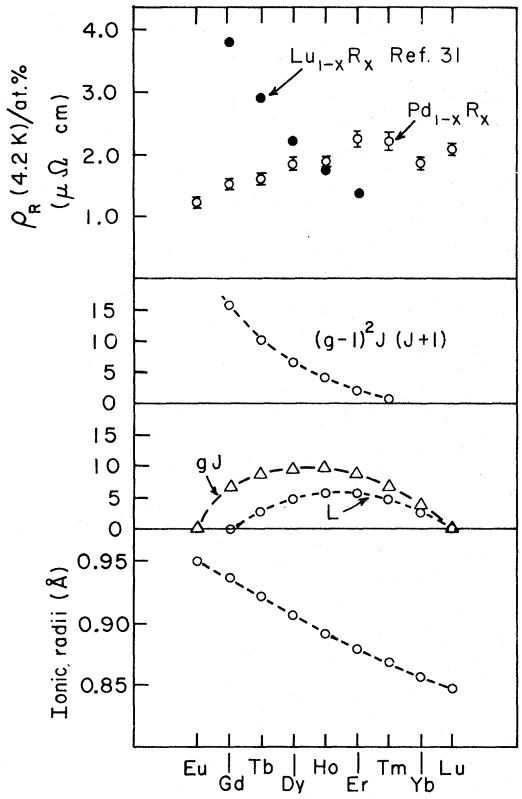

FIG. 10. Residual resistivity at 4.2 K due to 1 at.% rare earth, $\rho_R(4.2\ \mathrm{K})$, for the $Pd_{1-x}R_x$ alloys vs atomic number for R = Eu, Gd, Tb, Dy, Ho, Er, Tm, Yb, or Lu. The Pd matrix resistivity ($\sim 0.1\ \mu\Omega$ cm) has been subtracted from the measured resistivity. The error bars represent the $\pm 5\%$ variation of several measurements on the same alloys. Also plotted are the de Gennes factor $(g-1)^2J(J+1)$, the total orbital angular momentum L, the free-ion moment gJ, and the ionic radii for the heavy R^{3+} ions.

value of the angular momentum J of the rare-earth ion, $W = kT_0$ is an over-all scaling factor for H_{CF}, and $-1 \leq x \leq +1$ is related to the ratio $-\infty < B_4/B_6 < \infty$.

There are several ways to evaluate x and W: (a) from a fit of the magnetic-moment data, (b) from a fit of the anisotropy and g value of the EPR data, and (c) from a combination of both (a) and (b). We find that we cannot obtain a precise value of x and W by using only magnetic data. In principle the EPR data may be used to determine x (by employing an effective spin Hamiltonian) and then W may be determined from the magnetic data. Since 210 kG corresponds to an energy of about $28k_B$ for $g = 2$, we expect that the approach to saturation of the rare-earth ion will be strongly influenced by the crystal field splitting. Therefore we can determine W by fitting the $\sigma(H_0)$ data to the results of crystal field theory using the value of x obtained from the analysis of the EPR data. Dy was selected for this analysis since it is the only non-S-state rare-earth ion in Pd for which EPR data have been published.[5,30a] We have found that *both* W and x (for Dy) can be determined precisely from a proper analysis of the available EPR data alone. Here we have used these independently determined values of x and W in order to compare the magnetic-moment data with predictions of crystal field theory.

b. EPR in Pd(Dy) alloys. Recently Devine *et al.*[5] discussed the EPR of Dy^{3+} in single-crystal Pd. The spin-Hamiltonian analysis of the g value and the anisotropy of the most intense EPR line indicated $-0.6 < x < -0.2$ and $W < 0$. For this range of x and W, the ground state and the first

TABLE III. Summary of magnetic-moment vs field $[\sigma(H_0)]$ data to 200 kG at 4.2 K on $Pd_{1-x}R_x$ alloys. The parameters C, B, and A are determined from rms fit to Eq. (2). C is the band susceptibility, B is a measure of the ease of magnetic saturation (low B indicates a rare earth that is very difficult to saturate), and $p_{sat}(\propto A/B)$ is the moment of R. The term gJ is the moment expected for an R^{3+} ion (except Ce and Pr, which are R^{4+}).

Rare earth	Conc. (at.%)	C (10^{-6}/g)	B (10^6 G)$^{-1}$	$p_{sat}(\propto A/B)$ (μ_B/R atom)	gJ
Ce	0.06	6.87[a]		0	0
Ce	0.25	5.92[a]		0	0
Ce	0.67	5.54[a]		0	0
Ce	1.00	5.66[a]		$<10^{-3}$	0
Ce	1.57	4.63[a]		0	0
Ce	2.95	3.24[a]		0	0
Ce	6.7	1.71[a]		0	0
Pr	1.00	6.3	20	2.1	2.1
Nd	1.00	5.4	25	3.3	3.3
Nd	2.00	2.5	20	3.8	3.3
Sm	1.00	5.9	6	0.8	0.7
Eu	1.30	6.1[b]		0	0
Gd	0.29	5.6[b]	60	8.0	7
Gd	0.68	5.0[b]	90	7.5	7
Gd	1.00	4.6	100	7.2	7
Gd	1.38	4.8	130	7.1	7
Gd	2.03	3.6	160	6.8	7
Tb	1.00	4.8	85	9.0	9
Dy	0.25	6.7[b,c]	75	9.2	10
Dy	1.05	7.3	95	8.9	10
Dy	2.00	7.2	95	8.2	10
Ho	1.00	5.1	80	9.6	10
Er	0.10	5.4[b]	45	11.3	9
Er	0.20	5.4[b,c]	40	15.2	9
Er	1.00	4.2	65	9.5	9
Tm	1.50	5.5	45	6.0	7
Yb	0.85	4.9	20	4.4	4
Lu	0.50	6.55[a]		0	0
Lu	1.00	6.0[b]		0	0
Lu	1.89	5.05[a]		0	0
Y	1.50	4.7		0	0

[a] Measured at 4.2 K in fields to 50 kG.
[b] Measured at 4.2 K in fields to 140 kG.
[c] Arc-melted sample of Davidov *et al.* (Ref. 29).

excited set of energy levels are the $\Gamma_8^{(3)}$ and $\Gamma_8^{(2)}$ quartets.

We have reanalyzed the EPR data as follows: The 16×16 matrix of the cubic crystal field, suitable for the $J=\frac{15}{2}$ ground level of the $4f^9$ configuration of Dy^{3+}, including the interaction with an arbitrarily oriented magnetic field H_0, was diagonalized. We calculated the transition probability, weighted by the proper Boltzmann factor, for the six possible transitions between four levels for the $\Gamma_8^{(2)}$ and $\Gamma_8^{(3)}$ quartets. This was necessary in order to identify the strongest resonance. Surprisingly, we found that the anisotropy of the strongest EPR line could be used to determine uniquely the values of $T_0 = 89.3$ mK and $x = -0.5418$. This EPR line results from the transitions between the *second and third levels* of the ground-state quartet $\Gamma_8^{(3)}$, instead of between the first and second levels, as suggested by Devine *et al.*[5] In addition, the g factor is strongly magnetic field dependent. The over-all splitting of the multiplet is ~ 25 K and the next quartet, $\Gamma_8^{(2)}$, is ~ 2.5 K above $\Gamma_8^{(3)}$. The detailed results of this analysis will be presented in a separate paper.[30b]

c. Application to magnetic-moment data of Pd(Dy) alloys. Based on the unique determination of x and W described in Sec. IV B 2 b, we can proceed with the analysis of the magnetic-moment data.

The eigenvalues were used to calculate the thermodynamic free energy of the rare-earth ion. A numerical differentiation with respect to the applied field H_0 gave the numerical value for the magnetic moment of the rare-earth ion as a function of W (or T_0) and x, the magnitude and orientation of H_0, and the temperature.

Since the contribution to the alloy magnetic moment by the rare-earth ion is anisotropic and the measurements were made in disordered polycrystalline alloys, we performed a numerical average over the three orientations ⟨001⟩, ⟨111⟩, and ⟨110⟩, with suitable weight factors, in lieu of an integration over the unit sphere. This average was then compared with the measured magnetic moment. The magnetic moment is then written as

$$\sigma(H_0) = mf(H_0, T) + CH_0 \ , \tag{5}$$

where $f(H_0, T)$ can be calculated numerically as a function of H_0 and T, and m (which is proportional to the rare-earth concentration) and C are adjustable parameters for the rms fit to the measured moment.

The theoretical results were compared with the following experimental data: (i) the magnetic moment measured at constant field (2.2 kG) as a function of temperature, $4.2 \leq T \leq 250$ K, and (ii) the magnetic moment at constant temperature (4.2 K) as a function of applied field, $11 \leq H_0 \leq 210$ kG. For the discussion of the fit of Eq. (2) to the magnetic-moment data in Sec. IV B 1, we fixed the concentration and allowed p_{sat} and χ_{mat} to be adjustable parameters. When we employ crystal field theory, p_{sat} is fixed since the $^6H_{15/2}$ term of Dy^{3+} has a moment of $10\mu_B$. Furthermore, x and W are fixed by the analysis of the EPR data. The only adjustable parameter available to us is C. In order to obtain a better fit of theory to data, we have also allowed the concentration to be adjusted for comparison with the crystal field calculations.

The temperature dependence of the magnetic moment was examined for the 1.05-at. %-Dy alloy. The moment calculated from crystal field theory was normalized to the experimental data point at 68 K, where the rare-earth moment is approximately three times the host moment. From this normalization we calculate a rare-earth concentration $n' = 0.95$ at. %. We find good agreement between theory and experiment at $T > 35$ K, where the Curie law is well obeyed. For $T \leq 30$ K both theory and experiment deviate from the Curie law in the same direction, but the deviation of the experimental data points is two or three times larger.

The field dependence of the magnetic moment at 4.2 K was examined for both the 0.25- and 1.05-at. %-Dy alloys. The best rms fit to the experimental data gave

1.05 at. %Dy: $n'' = 0.86$ at. %, $C = 8.4\times10^{-6}$emu/g;

0.25 at. %Dy: $n'' = 0.20$ at. %, $C = 8.0\times10^{-6}$emu/g.

If we set $p_{sat} = 10\mu_B$/Dy atom, use the values of C taken from Table III, and allow only the concentration to be an adjustable parameter in Eq. (2), we obtain

1.05 at. %Dy: $n'' = 0.90$ at. %, $C = 7.3\times10^{-6}$emu/g;

0.25 at. %Dy: $n'' = 0.23$ at. %, $C = 6.7\times10^{-6}$emu/g.

The crystal field fit gives concentrations $n'' \sim 20\%$ below the nominal values and χ_{mat} is even larger than the susceptibility measured at 200 kG. Furthermore, the deviations between theory and experiment are systematic. The very large value of C is the result of an rms force fitting of the crystal field theory to experiment—the theoretical results approach saturation more rapidly than experiment and, to compensate for this, an unrealistically large value of C is required.

3. Comparison of Analyses of Magnetic-Moment Data

In Secs. IV B 1 and IV B 2 we discussed how both Eq. (2) and crystal field theory (CFT) were fitted

to the experimental $Pd_{1-x}Dy_x$ data. In this section we summarize the relative merits of each approach.

The rms error of the CFT fit to the magnetic-moment data of $Pd_{1-x}Dy_x$ is two or three times larger than the fit using Eq. (2). Unfortunately, this difference is not large enough to conclude that one method has a unique advantage over the other. Therefore, we must examine the fits in more detail.

We think it is significant that there are systematic deviations of the CFT fit; the theory predicts a too rapid approach to saturation of the Dy magnetic moment. As pointed out in Sec. IV B 2, in order to obtain the best rms fit an anomalously large matrix susceptibility was required. It should be noted that in the case of $Pd_{1-x}Gd_x$ CFT also predicts a too rapid saturation of the rare-earth magnetic moment (see Fig. 8). Here the magnetic moment should saturate as a $B_{7/2}$ Brillouin function, since Gd^{3+} is an S-state ion and only second-order fine-structure effects have been observed.[6] It is clear then that in order to fit the data using CFT further perturbations to the theory must be included in order to explain the slow approach to saturation observed in both $Pd_{1-x}Dy_x$ and $Pd_{1-x}Gd_x$. This perturbation should affect primarily the high-field magnetic properties, since it has already been pointed out that CFT adequately explains the low-field ($H_0 \lesssim 4$ kG) EPR data and the temperature dependence of the magnetic moment.

We have so far not considered the possibility that there may be concentration-dependent contributions to the parameters (W and x) of CFT. Dy concentrations of 100 and 500 ppm were used in the EPR measurements. These concentrations are too low for us to use for high-field magnetic-moment measurements; the Dy content of our alloys was much higher (0.25 and 1.05 at. %). We recognize the possibility that there may be rare-earth–rare-earth interactions and/or intermetallic compounds (e.g., Pd_3R) present in our more concentrated alloys. However, we find no evidence for the presence of the Pd_3R phase in our alloys (see Appendix A). We also examined the concentration dependence of the magnetic-moment isotherms at 4.2 K in the alloys of $Pd_{1-x}Gd_x$ ($x = 0.0029$, 0.01, and 0.02), $Pd_{1-x}Dy_x$ ($x = 0.01$, 0.0025), and $Pd_{1-x}Er_x$ ($x = 0.01$, 0.002, and 0.001). The rare-earth moments ($\sigma - \chi_{mat}H_0$) for each rare-earth system were normalized at $H_0 \sim 50$ kG and compared. We find that for $Pd_{1-x}Dy_x$ and $Pd_{1-x}Er_x$ the normalized data fall on the same curve to within experimental error (2%). In this procedure χ_{mat} is obtained from Table III for $x > 0.0025$, and $\chi_{mat} = \chi_{Pd}$ was used for the more dilute alloys. These results show that there are no discernible concentration-dependent effects on $\sigma - \chi_{mat}H_0$ for these alloys.

In order to examine the applicability of CFT in greater detail, magnetic measurements in single-crystal $Pd_{1-x}R_x$ alloys would be valuable. So far these materials have not been available to us.

Whether or not CFT is applicable to the $Pd_{1-x}R_x$ alloys, Eq. (2) provides a convenient way of describing the measured results, particularly when it is necessary to analyze a large amount of data. In contrast, CFT requires a lengthy and time-consuming numerical analysis as well as independent experimental results and analysis (e.g., EPR or neutron scattering). Finally, the CFT analysis of the data for $Pd_{1-x}Dy_x$ and $Pd_{1-x}Gd_x$ gives values of the matrix susceptibility and saturation moment per rare-earth atom that are not satisfactory. Equation (2) provides more reliable values of these quantities (see Table III).

V. LOW-TEMPERATURE RESISTIVITIES

The low-temperature electrical resistivities of the $Pd_{1-x}R_x$ alloys for $x \sim 0.01$ were measured in an attempt to correlate the rare-earth–conduction-electron scattering with the bulk magnetic properties. The resistivity is very sensitive to the atomic size and the charge distribution as well as the magnetic moment of the rare-earth ion.

A. Experimental Results

Most of the resistivity measurements were taken at 4.2 K. In the case of $Pd_{1-x}Gd_x$ and $Pd_{1-x}Ce_x$ the temperature dependence of the resistivity was measured for $1.5 \lesssim T \lesssim 20$ K and the resistivity was independent of T to about one part in 1000 for $T \lesssim 10$ K. We assume that the different scattering mechanisms are additive and that the excess resistivity per at. % rare-earth ion is given by $\rho_R(T) = [\rho(T) - \rho_{Pd}(T)]/100x$, where $\rho(T)$ is the measured resistivity of the alloy and $\rho_{Pd}(T)$ is our measured resistivity of pure Pd. The resistivity of Pd (~ 0.1 $\mu\Omega$ cm) is less than 10% of the total resistivity in all cases and $\rho(T)$ is primarily due to scattering from the rare-earth ions.

In Table IV we tabulate the values of $\rho(4.2\text{ K})$ obtained for the $x \sim 0.01$ $Pd_{1-x}R_x$ alloys discussed in the previous sections. The method of measurement was outlined in Sec. II C. All the data were normalized to $x = 0.01$. In all cases at least two measurements of $\rho(4.2\text{ K})$ were made on different pieces of the same alloy, and these measurements never differed by more than ± 5%. These variations in $\rho(4.2\text{ K})$ include effects of incomplete annealing and/or accidental cold working after the anneal.

In what follows we will confine our discussion to the data for the heavy rare-earth alloys ($Pd_{1-x}Eu_x$ through $Pd_{1-x}Lu_x$). The light rare-earth

TABLE IV. Residual resistivities $\rho(4.2\ \mathrm{K})$ per at. % rare earth of the $Pd_{1-x}R_x$ alloys. The term $(g-1)^2J(J+1)$ is the de Gennes factor for R^{3+} rare earths. Also listed for the heavy rare-earth alloys are the total-orbital-angular-momentum quantum number L and the free-ion moment gJ.

R	$\rho(4.2\ \mathrm{K})$ ($\mu\Omega$ cm)/at. %	$(g-1)^2J(J+1)$	L	gJ
$Ce^{(4+)}$	1.72			
$Pr^{(4+)}$	0.86			
Nd	1.38			
Sm	2.42			
Eu	1.36			
Gd	1.63	15.75	0	7
Tb	1.71	10.50	3	9
Dy	1.97	7.08	5	10
Ho	1.93	4.50	6	10
Er	2.33	2.55	6	9
Tm	2.30	1.17	5	7
Yb	1.92	0.32	3	4
Lu	2.12	0	0	0

data will not be considered because they are incomplete, the Ce and Pr ions are quadrivalent in Pd (see Sec. IV), and finally the anomalously large value of $\rho(4.2\ \mathrm{K})$ for $Pd_{1-x}Sm_x$ is not understood.

In Fig. 10 we show the values of the resistivity per at. % rare earth, $\rho_R(4.2\ \mathrm{K})$, for the heavy rare-earth alloys. The error bars represent the $\pm 5\%$ variation in the data. The data of MacKintosh and Smidt on $Lu_{1-x}R_x$ alloys[31] are also shown in Fig. 10. The lower portions of Fig. 10 show the de Gennes factor $(g-1)^2J(J+1)$, the free-ion moment gJ, the total orbital angular momentum L, and the ionic radii for the trivalent rare-earth ions.

B. Discussion

1. $Lu_{1-x}R_x$ Alloys (MacKintosh and Smidt)

As seen in Fig. 10, the data for the $Lu_{1-x}R_x$ alloys are strikingly different from those of our $Pd_{1-x}R_x$ alloys. The values of $\rho_R(4.2\ \mathrm{K})$ for the $Lu_{1-x}R_x$ system are closely proportional to the de Gennes factor plotted in Fig. 10. Thus these data obey the Kasuya formula[32] of magnetic impurity resistivity given by

$$\rho_R(0) = Kx[A^2(0) + J_{sf}^2(g-1)^2J(J+1)] \quad . \tag{6}$$

In interpreting the $Lu_{1-x}R_x$ data it is assumed that $A(0)$ (proportional to the Coulomb scattering) and J_{sf} (conduction-electron–$4f$-electron exchange parameter) are constants for all these alloys. This model is based on the premise that the rare-earth moments are well localized and have $2J+1$ degenerate ground-state levels available for magnetic exchange scattering with the conduction electrons.

It is clear from Fig. 10 that the $\rho_R(4.2\ \mathrm{K})$ for the $Pd_{1-x}R_x$ alloys does not obey the Kasuya formula.

2. $Pd_{1-x}R_x$ Alloys

The features of the $Pd_{1-x}R_x$ data in Fig. 10 suggest that ρ_R is a sum of three factors: a constant term, a term that increases linearly with the atomic number of the rare-earth ion, and a term which is zero for $Pd_{1-x}Eu_x$ and $Pd_{1-x}Lu_x$ and is maximum near $Pd_{1-x}Er_x$. The constant term, which is the largest contribution to ρ_R, is attributed to Coulomb scattering from the spherical charge distribution of the rare-earth ion. The term that increases linearly with the atomic number is attributed to differences in the rare-earth ionic radii relative to the metallic radius of the host. The ionic radii decrease linearly with atomic number (see Fig. 10). Since the metallic radius of Pd is larger than the ionic radius of any of the rare earths, the perturbation to the periodicity of the lattice should increase with increasing atomic number.[33] The third term is zero unless the rare-earth ion has a magnetic moment; it will be discussed in more detail below.

The excess resistivity ρ_R then can be expressed by

$$\rho_R = a + bn + \rho_R' \quad . \tag{7}$$

The values of a and b may be obtained from the resisitivites of $Pd_{1-x}Eu_x$ and $Pd_{1-x}Lu_x$ (neither Eu nor Lu has a moment in Pd). The integer n is the number of electrons in the $4f$ shell of the R^{3+} in $Pd_{1-x}R_x$ where $n = 6, 7, \ldots, 14$. The term ρ_R' in Eq. (7) is shown in Fig. 11. It is clear from Fig. 11 that ρ_R' is more nearly proportional to L or gJ than to the de Gennes factor (cf. Fig. 10).

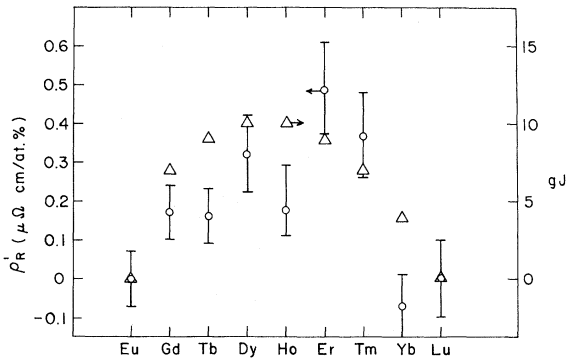

FIG. 11. Resistivity ρ_R' (see open circles) at 4.2 K of the $Pd_{1-x}R_x$ alloys for R = Eu, Gd, Tb, Dy, Ho, Er, Tm, Yb, or Lu after subtraction of the potential scattering [see Eq. (7)]. The error bars represent the $\pm 5\%$ variation of several measurements of the 4.2 K resistivity on the same samples. The triangles represent the free-ion moment gJ for the R^{3+} ions (see right-hand scale) and show the rough proportionality between ρ_R' and the free-ion moment.

A variation of ρ_R' with L might be expected if Coulomb scattering from the nonspherical part of the $4f$ charge distribution is important in these alloys. This effect was discussed by Fulde *et al.*,[34] who pointed out that aspherical Coulomb scattering is strongest when the conduction electrons have a large d-like character. This may be important for Pd, which has a large d-band density of states at the Fermi surface. However, we have no way of evaluating the strength of the aspherical Coulomb scattering from first principles or from independent experimental evidence.

The ρ_R' terms also may be produced by conduction-electron scattering from the magnetic dipole moment of the rare-earth ion. A moment which responds as a free ion to a magnetic field should produce conduction-electron scattering by the free ion resulting in a resistivity given by the de Gennes factor in Eq. (6). For a less responsive moment, ρ_R' should be better characterized by scattering from a more nearly fixed magnetic dipole moment. For a rare-earth magnetic moment with a fixed orientation, ρ_R' would be given by

$$\rho_R' = c(g_J J) \ . \tag{8}$$

From the field dependence of the rare-earth moment for all the $Pd_{1-x}R_x$ alloys, we conclude that the rare-earth moment in Pd is less responsive to a magnetic field than a free ion. Therefore we would expect ρ_R' to be more nearly proportional to $g_J J$ rather than the de Gennes factor in Eq. (6). This appears to be the case; the term $g_J J$ is also plotted (see triangles) in Fig. 11 for comparison.

In contrast, the data of MacKintosh and Smidt[31] showed that ρ_R' was proportional to the de Gennes factor for $Lu_{1-x}R_x$. From the above discussion the rare-earth moments in these alloys appear to behave as nearly free ions. Although no magnetic-moment data are available for these alloys, we would expect that the field dependence of the rare-earth moment would follow closely a Brillouin function.

ACKNOWLEDGMENTS

We would like to thank Professor R. Orbach and Dr. D. Davidov for useful discussions about the EPR of rare-earth ions in metals and for furnishing several splat-cooled alloys. Also, we wish to thank E. J. Alexander and W. Martin for valuable technical assistance.

APPENDIX A: SEARCH FOR Pd_3R PHASE IN $Pd_{1-x}R_x$ ALLOYS

The results of x-ray studies on the $Pd_{1-x}Gd_x$ alloys were presented in Sec. II. No evidence of the Pd_3Gd phase was found for $x \lesssim 0.05$.

A striking resistive maximum was observed[35] for Pd_3Gd: $\rho(T)$ increased by ~ 30% from 4 K to a maximum at 8 K, then decreased to a shallow minimum at 10 K, and finally increased monotonically with increasing temperature. The $\rho(T)$ data of Schiffrin[36] on a $Pd_{0.911}Gd_{0.089}$ alloy showed a similar resistive anomaly, which we attribute to the presence of Pd_3Gd in his sample. We carefully examined the electrical resistivity of our $Pd_{0.99}Gd_{0.01}$ alloy for $4.2 \lesssim T \lesssim 20$ K. The resolution of our $\rho(T)$ data was better than $1:10^4$. No $\rho(T)$ anomaly was detected: $\rho(T)$ was constant up to ~ 8 K and then increased monotonically up to 20 K. We conclude that any Pd_3Gd phase, if present, constitutes less than ~ 0.03% of this sample. Since for most of our samples $x \lesssim 0.01$, we assume that the Pd_3R intermetallic phase is negligible in our $Pd_{1-x}R_x$ alloys.[37]

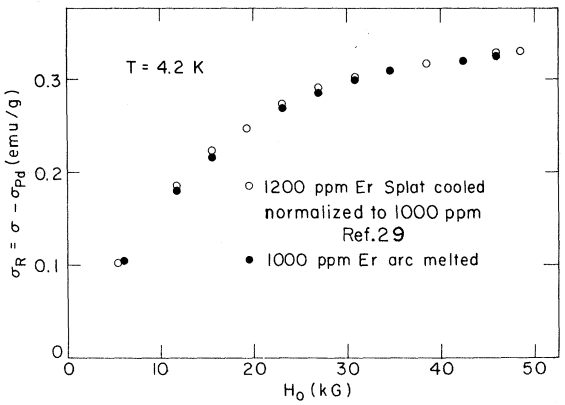

FIG. 12. Comparison of the magnetic-moment data at 4.2 K of a 1200-ppm Er-in-Pd splat-cooled alloy with a 1000-ppm Er-in-Pd arc-melted alloy. The data of the splat-cooled alloy are normalized to 1000-ppm Er. Any variation in the magnetic properties of alloys prepared in different ways for this concentration range is within experimental error.

APPENDIX B: COMPARISON OF ARC-MELTED ALLOY WITH SPLAT-COOLED ALLOY

We have compared the magnetic moment of a splat-cooled 1200-ppm Er-in-Pd alloy of Davidov *et al.*[29] with our arc-melted 1000-ppm Er-in-Pd alloy. The magnetic moment vs H_0 per 1000-ppm Er for both alloys at 4.2 K is shown in Fig. 12. Here we assumed that $\chi_{mat} = \chi_{Pd}$ ($= 6.7 \times 10^{-6}$ emu/g). The normalized data agree within 2% up to 50 kG. We conclude that the magnetic properties of the $Pd_{1-x}R_x$ alloys in the $x \sim 0.001$ concentration range are identical for both methods of preparation.

*Work supported by the U. S. Air Force Office of Scientific Research and the National Science Foundation.

†Visiting scientist at the Francis Bitter National Magnet Laboratory, Massachusetts Institute of Technology, Cambridge, Mass. 02139.

‡Partially supported by a grant from the Research

Corp.

§Now supported by the National Science Foundation.

[1]D. Shaltiel, J. H. Wernick, H. J. Williams, and M. Peter, Phys. Rev. 135, A1346 (1964).

[2]M. Peter, D. Shaltiel, J. H. Wernick, H. J. Williams, J. B. Mock, and R. C. Sherwood, Phys. Rev. 126, 1395 (1962).

[3]J. Crangle, Phys. Rev. Letters 13, 569 (1964).

[4]D. Davidov, R. Orbach, C. Rettori, D. Shaltiel, L. J. Tao, and B. Ricks, Solid State Commun. 10, 451 (1972); E. P. Chock, R. Chui, D. Davidov, R. Orbach, D. Shaltiel, and L. J. Tao, Phys. Rev. Letters 27, 582 (1971); D. Davidov, R. Orbach, L. J. Tao, and E. P. Chock, Phys. Letters 34A, 379 (1971).

[5]R. A. Devine, J.-M. Moret, J. Ortelli, D. Shaltiel, W. Zingg, and M. Peter, Solid State Commun. 10, 575 (1972).

[6]R. A. Devine, D. Shaltiel, J.-M. Moret, J. Ortelli, P. Donze, and M. Peter, Solid State Commun. 11, 525 (1972).

[7]R. P. Guertin, S. Foner, E. J. McNiff, Jr., and H. C. Praddaude, J. Appl. Phys. 42, 1550 (1971).

[8]H. C. Praddaude, S. Foner, E. J. McNiff, Jr., and R. P. Guertin, in *Magnetism and Magnetic Materials*, edited by H. Wolfe (AIP, New York, 1972).

[9]M. P. Sarachik, J. Appl. Phys. 38, 1155 (1967).

[10]S. Arajs, G. R. Dunmyre, and S. J. Dechter, Phys. Status Solidi 18, 505 (1966).

[11]H. C. Praddaude, Phys. Letters 34A, 281 (1971).

[12]K. A. Gschneidner, Jr. (private communication).

[13]J. Crangle and R. B. Layng, STAR; 4, 1742 (1966); AD627224 CFSTI (available from U.S. Government Clearinghouse).

[14]I. R. Harris and G. V. Raynor, J. Less Common Metals 9, 263 (1965).

[15]S. Foner, Rev. Sci. Instr. 30, 548 (1959).

[16]S. Foner and E. J. McNiff, Jr., Rev. Sci. Instr. 39, 171 (1968).

[17]J. W. Loram, P. J. Ford, and T. E. Whall, J. Phys. Chem. Solids 31, 763 (1970).

[18]See, for example, D. S. McClure, in *Electronic Spectra of Molecules and Ions in Crystals*, edited by F. Seitz and D. Turnbull (Academic, New York, 1959).

[19]G. Williams and L. L. Hirst, Phys. Rev. 185, 407 (1969).

[20]R. Doclo, S. Foner, and A. Narath, J. Appl. Phys. 40, 1206 (1969).

[21]F. E. Hoare and J. C. Matthews, Proc. Roy. Soc. (London) A212, 137 (1952).

[22]A. B. Lidiard, Proc. Roy. Soc. (London) A224, 161 (1954).

[23]E. W. Elcock, P. Rhodes, and A. Teviotdale, Proc. Roy. Soc. (London) A221, 53 (1954).

[24]J. Crangle and T. F. Smith, Phys. Rev. Letters 9, 86 (1962).

[25]M. Shimizu, T. Takahashi, and A. Katsuki, J. Phys. Soc. Japan 18, 240 (1963).

[26]S. Misawa, Phys. Letters 32A, 541 (1970).

[27]S. Doniach, Proc. Roy. Soc. (London) 91, 86 (1967).

[28]S. Foner and E. J. McNiff, Jr., Phys. Letters 29A, 28 (1969).

[29]D. Davidov, R. Orbach, C. Rettori, D. Shaltiel, L. J. Tao, and B. Ricks, Solid State Commun. 10, 451 (1972); also D. Davidov (private communication).

[30]K. R. Lea, M. J. M. Leask, and W. P. Wolf, J. Phys. Chem. Solids 23, 1381 (1962).

[30a]Recently EPR of Er has been observed in single crystal Pd; see R. A. B. Devine, W. Zingg, and J.-M. Moret, Solid State Commun. 11, 233 (1972).

[30b]H. C. Praddaude, Phys. Letters A (to be published).

[31]A. R. MacKintosh and F. A. Smidt, Jr., Phys. Letters 2, 107 (1962).

[32]T. Kasuya, Progr. Theoret. Phys. (Kyoto) 22, 227 (1959).

[33]We assume that the metallic radius of Pd is appropriate here rather than the ionic radius since the 4*d* electrons of Pd are largely localized.

[34]P. Fulde, L. L. Hirst, and A. Luther, Z. Physik 230, 155 (1970).

[35]R. D. Hutchens, V. S. Rao, J. E. Greedon, W. E. Wallace, and R. S. Craig, J. Appl. Phys. 42, 1293 (1971).

[36]A. M. Schiffrin, Phys. Status Solidi 39, K81 (1970).

[37]We have also measured $\rho(T)$ of several $Pd_{1-x}Ce_x$ alloys (see Table III) for $0.01 \lesssim x \lesssim 0.06$ and $4.2 \lesssim T \lesssim 20$ K. No resistive minima or maxima were detected in this temperature range; $\rho(T)$ was constant to $\sim 1:10^4$ for $T \lesssim 10$ K and increased monotonically with T to 20 K.